A hybrid intelligent classifier to estimate obesity levels based on ERG signals

İrem Senyer Yapici [a,*], Okan Erkaymaz [b], Rukiye Uzun Arslan [a]

[a] *Department of Electrical and Electronics Engineering, Zonguldak Bülent Ecevit University, Zonguldak, Turkey*
[b] *Department of Computer Engineering, Zonguldak Bülent Ecevit University, Zonguldak, Turkey*

ARTICLE INFO

ABSTRACT

Obesity is a worldwide prevalence metabolic disease causing significant eye problems. Body Mass Index is proved to not be a sufficient criterion to classify obesity. In this context, a diagnostic support system for determining obesity levels by using electroretinogram signals is designed. To do this, the discrete wavelet transform is applied to three different electroretinogram responses recorded from both eyes. The obtained wavelet coefficients' size is reduced using statistical property. The designed dataset is used in artificial neural networks and artificial neural networks based particle swarm optimization models to classify obesity. We found that the average accuracy of the hybrid model is higher than the traditional model and the cone response is a highly effective response in obesity classification. This study is the first attempt to classify obesity levels based on electroretinogram signals and this study shows that obesity can be classified from electroretinogram signals.

1. Introduction

Obesity, described by abnormal or excessive fat accumulation, is a major health problem of the developed and developing countries nowadays. In the outpatient clinic, body mass index (BMI) is a mostly preferred measurement method to classify obesity. BMI is defined as the ratio of the body weight in kilograms to the square of the height in meters [1,2]. In accordance with World Health Organization (WHO)'s quality standards, commonly accepted BMI ranges are normal, 18-25 kg/m^2; overweight, 25-30 kg/m^2; obese, 30-40 kg/m^2; morbid obese, 40-50 kg/m^2; and super obese, greater than 50 kg/m^2 [3]. It has been found out that obesity has long been associated with major negative health outcomes such as cardiovascular disease, diabetes, depression, stroke, and even cancer [4–10]. Besides, the deleterious influences on vision system of obesity lead to great variety of eye diseases including cataract, glaucoma and macula [11–27].

On the other hand, ophthalmic electrophysiology tests such as Electrooculography (EOG), Electroretinography (ERG) and Visual evoked potential (VEP) are frequently used by ophthalmologists in the early diagnosis of eye diseases [28–32]. Among them, ERG shows mass response of the retina consisting light-sensitive cells (rod cells, cone cells and ganglion cells) to an uniform flash light

[33,34]. It provides general information about retinal function and can reveal the functions of various cell types. Besides, it is a valuable diagnostic tool for diagnosing, monitoring and evaluating the effectiveness of therapeutic interventions for retinal diseases [35–38]. The interpretation of ERG signals is commonly performed by using five ERG responses (rod response, cone response, maximal combined response, 30 Hz flicker response and oscillatory potentials) defined by ISCEV (International Society for Clinical Electrophysiology of Vision) standards. Within the scope of this study, rod response, cone response and maximal combined response have been used. Rod response recorded from rod cells is defined as the first signal observed after dark adaption. The maximal combined response is measured from rod and cone cells in the dark-adapted eye. Cone response is obtained from the cone cells after brightening adaptation is achieved [39,40].

Furthermore, the importance of decision support systems in medicine has been increasing day by day. These systems are a powerful tool for specialist physicians to diagnose diseases at early stage. In this context, in many studies, ERG signals have been utilized for classifications based machine learning and data mining algorithms conducted for the diagnosis of eye diseases [31,41–48]. For example, Guven et al. proposed a diagnostic method based traditional artificial neural network (ANN) to detect macular diseases by using pattern ERG (PERG) signals [41]. Polat et al. suggested a hybrid automatic detection system based k nearest neighbor and support vector machine techniques to classify macular disease using PERG signals [43]. Miguel-Jimenez et al. classified glaucoma

* Corresponding author.
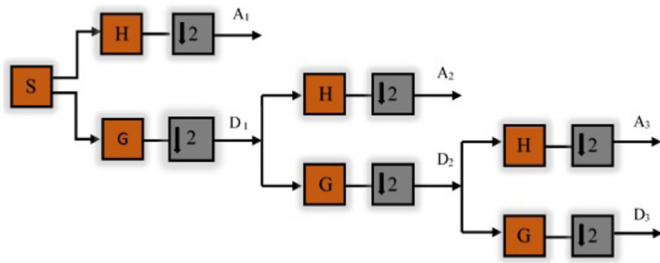*E-mail address:* senyerirem@beun.edu.tr (İ.S. Yapici).

İ.S. Yapici, O. Erkaymaz and R.U. Arslan

Fig. 1. The general block diagram of the proposed automated decision support system model.

Fig. 2. Three-level discrete wavelet decomposition.

by combining the properties extracted from the multifocal ERG (mfERG) signals by structural model analysis with radial-based artificial neural networks [31]. Boquete et al. preferred radial-based artificial neural networks with extreme learning algorithm to diagnose glaucoma by usage of morphological properties of mfERG signals [45]. Bagheri et al. used empirical mode approach and ANN to make diagnosis of the retinal diseases from ERG signals [46].

Literature surveys indicate that BMI alone is not sufficient to measure a person's body composition [49–51]. Therefore, in a recent study, the effects of obesity on two main components ('a' and 'b' waves) of ERG signals are analyzed by Erkaymaz et al. They have analyzed the amplitudes and formation times of the waves based on statistical, time and time-frequency analysis for all obese groups. They have showed that the continuous wavelet transform is more successful to detect the effect of obesity classes on the waves [40]. On the other hand, to our knowledge, the classification of obesity levels based ERG signals has not been handled in studies conducted so far. Therefore, in this study, an automated decision support system model has been proposed and the classification of obesity has been performed by usage of three different ERG responses (rod, cone and maximal combined responses).

The rest of the paper is organized as follows. Section 2 briefly gives information about the ERG data acquisition, pre-processing, feature extraction and methods used for classification. The results are introduced in Section 3, followed by the conclusion and discussion.

2. Models and methods

In this section, the ERG data acquisition, pre-processing and feature extraction methods used in the proposed automated decision support system have been mentioned in detail. The general block diagram of the proposed system is illustrated in Fig. 1.

2.1. ERG dataset

The experimental study has been performed with forty-seven volunteers, aged between 18–70, with normal, overweight, obese, morbid obese and super obese. Before the enrollment of the study, a written informed consent is provided from each volunteer approved by the local ethics committee at Zonguldak Bulent Ecevit University. The experimental studies are performed in accordance with ISCEV standards and all essential explanations about the experimental procedure are given to the volunteers in advance. Furthermore, ophthalmological examinations of each volunteer are checked by an ophthalmologist.

ERG signals have been recorded in a well-equipped laboratory with the electrooculography "Metrovision MonPackOne" supplied by Zonguldak Bulent Ecevit University Scientific Research Project. Data acquisition considering ISCEV standards has been realized by using Dawson-Trick-Litzkow plus (DTL), reference and ground electrodes placed into the lower conjunctival sac of previously each dilated eyes, the sides and center of the forehead, respectively.
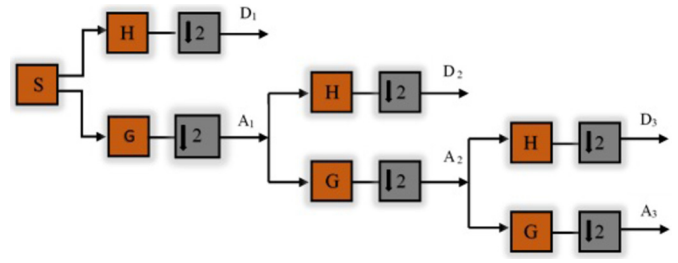
Then, firstly, the electrical responses of both eyes towards the light stimuli have been recorded by adopting 20 minute dark adaptation period. Same procedures have been repeated after 15 minutes of light adaptation; and hereby, the necessary recordings have been taken. Thus, the dataset recorded from forty seven volunteers has been created.

2.2. Feature extraction

2.2.1. Discrete Wavelet Transform (DWT)

The DWT is a powerful time-frequency tool for analyzing non-stationary signals such as biomedical signals. Because of its low computational cost and easy usability, the DWT has been frequently utilized in classification problems of biomedical signals to extract the required features [52]. In this method, signals are decomposed into a set of wavelets that are obtained by using low and high pass filters, based on the coefficients described below:

$$A_{j,k} = \sum_l g_{l-2k} A_{j-1,l} \tag{1}$$

$$D_{j,k} = \sum_l h_{l-2k} A_{j-1,l} \tag{2}$$

where j is the level of the transformation, k is the total number of coefficients, $A_{j,k}$ and $D_{j,k}$ represents the scaling and wavelet coefficients, respectively. g and h, in turn, denotes low pass filter and high pass filter coefficients of scaled and wavelet functions depending on a given wavelet type; and l represents the width of the filters [53–56]. Fig. 2 shows a three level DWT decomposition. The high frequency components of the raw signals are removed by the low-pass filters, and thus approximation coefficients (A_j) are obtained. On the other hand, high pass filters remove the low frequencies of the raw signal to detect detail coefficients. Hereby, the raw signal is separated to a shifted and scaled version of a chosen wavelet type obtained at level L. At each level, the obtained scaled and wavelet coefficients are sampled down by two, and thus series half the length of the filtered series are acquired. The repetition of the process is terminated as the desired wavelet decomposition level is reached [3,55,56].

In DWT, the choice of wavelet type is great of importance due to having different properties of each. Haar, Morlet, Mexican hat and Daubechies wavelets are some popular wavelet types. In this study, the extraction of ERG signals into sub-bands has been carried out by using a four level DWT with fourth-order Daubechies (db4) wavelet type that is widely utilized for biomedical signals in literature.

2.2.2. Statistical features

The dimensions of the coefficients extracted from DWT are reduced by applying the six different statistical properties listed in Table 1: the mean absolute value (μ), average power (λ), standard deviation (σ), skewness (ϕ), kurtosis (φ) of the signal coefficients in every sub-band and ratio of the absolute mean (χ) values of signal coefficients of adjacent sub-bands [57,58].

Table 1
Features and their equations.

Feature	Equations
μ	$\mu = \frac{1}{M} \sum_{j=1}^{M} |y_j|$
λ	$\lambda = \sqrt{\frac{1}{M} \sum_{j=1}^{M} y_j^2}$
σ	$\sigma = \sqrt{\frac{1}{M} \sum_{j=1}^{M} (y_j - \mu)^2}$
ϕ	$\phi = \sqrt{\frac{1}{M} \sum_{j=1}^{M} \frac{(y_j - \mu)^3}{\sigma^3}}$
φ	$\varphi = \sqrt{\frac{1}{M} \sum_{j=1}^{M} \frac{(y_j - \mu)^4}{\sigma^4}}$
χ	$\chi = \frac{\sum_{j=1}^{M} |y_j|}{\sum_{j=1}^{M} |z_j|}$

2.2.3. Artificial Neural Network (ANN)

ANN is a topology inspired from the biological brain networks, it consists of adaptive units (neurons) and interconnections associated with synaptic weights between neurons. In creating ANN architecture, these neurons are connected as feed forward or backward and thus, different ANN topologies can be obtained. Multilayer perceptron (MLP) is one of the basic and commonly used ANN topology in the literature [59]. In MLP, each neuron is connected to other neurons by means of directed feed forward communication links between layers. The MLP is generally composed with three layers: input, output and hidden layers. In the training process of MLP, the error propagated as backward is obtained by the knowledge transmitted between layers. This processing is iterated up to approach the desired output with minimum error by using different learning algorithms such as back-propagation, Quasi-Newton and Levenberg-Marquardt [60]. In this study, we designed a MLP topology with one hidden layer and the designed topology is trained by using Levenberg-Marquardt algorithm. The number of neurons in the hidden layer is determined from 8 to 20 neurons by performing 100 trials with a minimum error criterion (MSE).

2.2.4. Artificial Neural Network based Particle Swarm Optimization (ANN-PSO)

ANN is commonly a tool used for regression and classification with high generalization capability. Therefore, it is preferred especially to classify complex (nonlinear) biomedical signals [61–66]. The main advantage of ANN is easy to use and low computational cost. They have also ability to detect complex relationship maps between inputs/outputs in nonlinear signals. On the other hand, needing more training data, slow training process and overfitting problem are the major disadvantages. To overcome these disadvantages, a particle swarm optimization (PSO) based approach is used in proposed ANN model. The designed ANN-PSO model consists of traditional MLP architecture, whose parameters are calculated with PSO algorithm. The statistical features obtained from feature extraction process are provided as input to the model. The designed ANN model has three layers: an input layer, a hidden layer and an output layer. The model has a 29-H–1 network topology, where H defines the number of the hidden neuron. We apply training process on the model with 100 trials by using $H = 8, 10, \ldots, 20$ to determine the number of the neurons in the hidden layers. The obtained ANN architecture's parameters (weights and biases) are used in PSO algorithm.

PSO is the most popular swarm (population) intelligence algorithm, inspired from the social behavior of animals searching for food such as bird flocking or ant colonies. PSO performs optimization by a particle swarm which is updated at each iteration for each time-step. Each particle shifts towards the direction of its own history best position and global best position, to converge and acquire the global optimum. The mathematical expression of updated velocity and position vectors of particles are as follows:
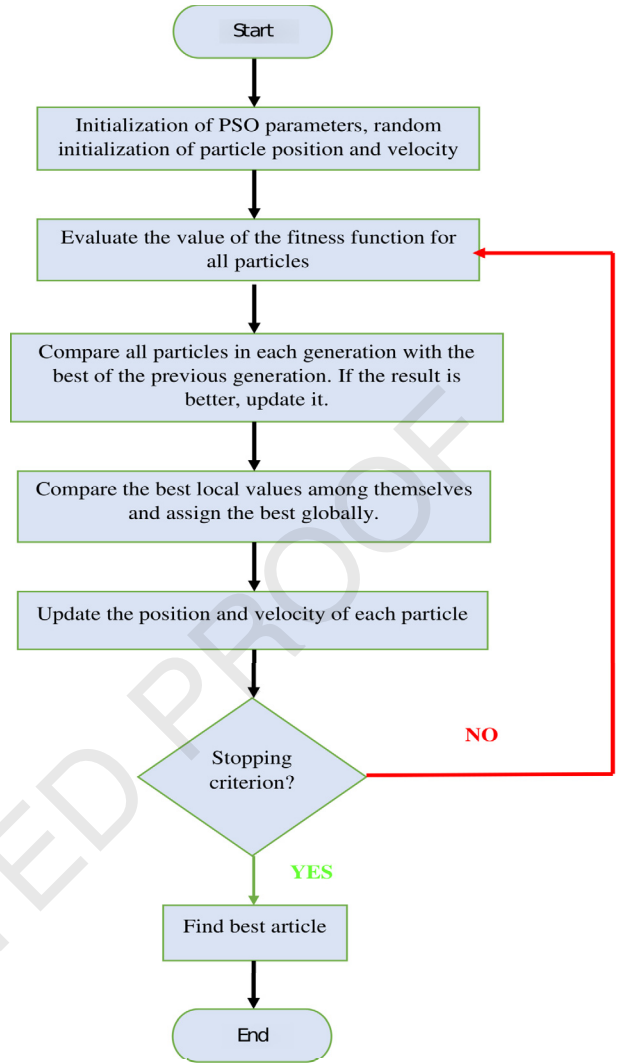

Fig. 3. Three-level discrete wavelet decomposition.

$$V_{i,d}(k+1) = W^* V_{i,d}(k) + c_1^* r_1^* (X_{pbest}(k) - X_{i,d}(k)) + c_2^* r_2^* (X_{gbest}(k) - X_{i,d}(k)) \quad (3)$$

$$X_{i,d}(k+1) = X_{i,d}(k) + V_{i,d}(k+1) \quad (4)$$

where $V_{i,d}(k)$ and $X_{i,d}(k)$ denote the velocity and position vectors of the "d"th dimension of "i"th particle at the "k"th iteration, respectively [67]. X_p best represent the p best position of the particle i, whereas X_g best gives the g best position of the population. W is the inertia weight which is used for balancing global and local values. The acceleration coefficients (c_1 and c_2) are used to control the effects of pbest and gbest on the new velocity and are tuned to 2. r_1 and r_2 are random numbers in the range of [0, 1]. b denotes the constraint factor that control the weight of the velocity. In the model, each particle is defined by the parameters w and b. Fig. 3 shows the flowchart of an ANN-PSO algorithm.

2.2.5. The performance measures

The performance of studies based on machine learning techniques have been evaluated by using diverse methods, such as resubstitution method, hold out method and leave one out method [3]. Within this study, the hold out method has been used. In this context, the data set is independently and randomly divided into two groups as training (80%) and testing (20%). Then, statistical measurements namely accuracy (ACC), sensitivity (SEN) and specificity (SPE) are calculated from confusion matrix for benchmarking
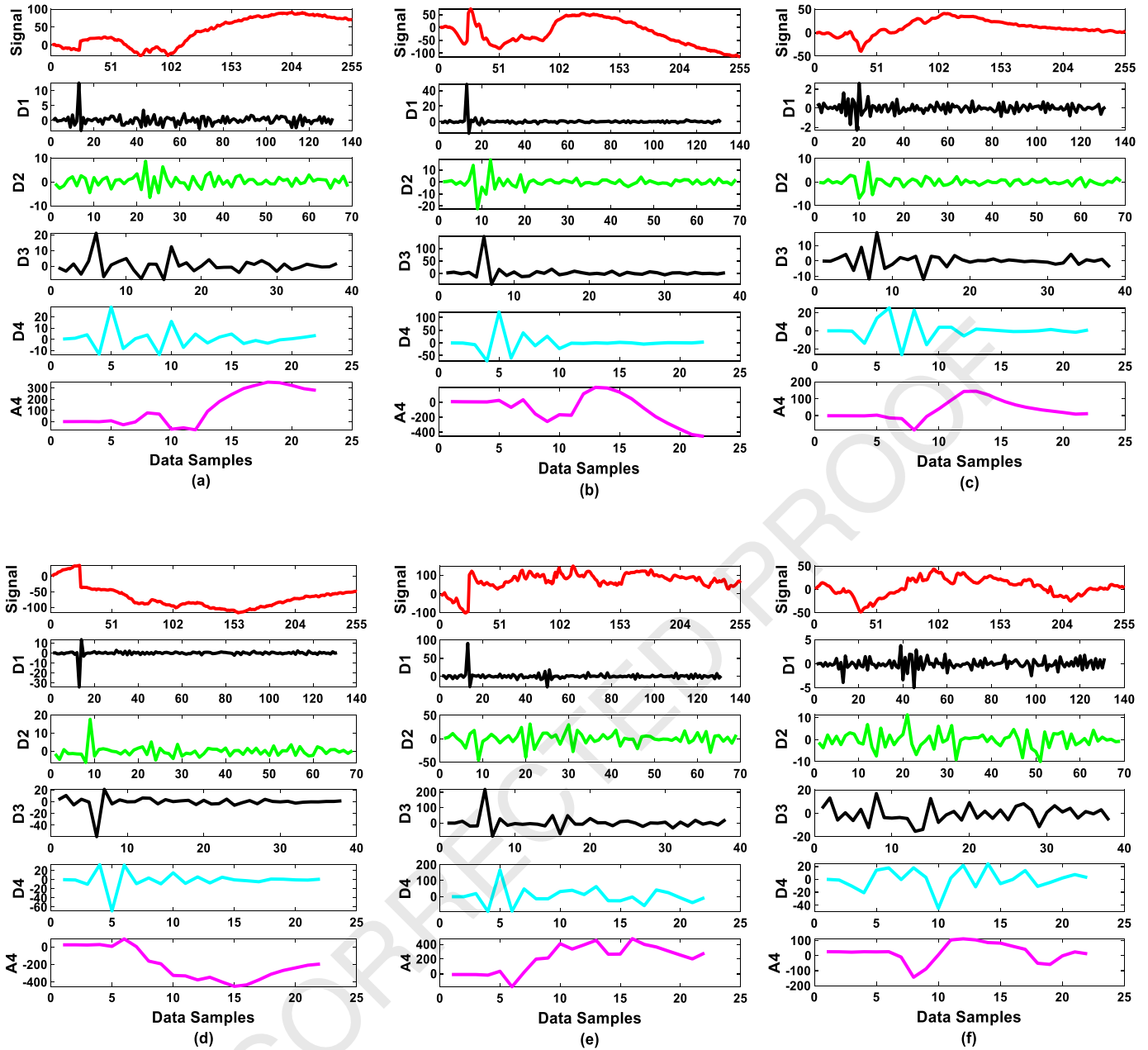
İ.S. Yapici, O. Erkaymaz and R.U. Arslan

Physics Letters A ●●● (●●●●) ●●●●●●

Fig. 4. The DWT coefficients obtained from fourth-level Daubechies wavelet (db4) of normal ERG signal; (a) rod response of the right eye, (b) maximal combined response of the right eye, (c) cone response of the right eye, (d) rod response of the left eye, (e) maximal combined response of the left eye, (f) cone response of the left eye.

designed models. SEN gives the ratio correctly classified samples to the total number of positive samples, whereas SPE is the ratio of correctly classified negative samples to the overall negative sample's count. ACC gives the proportion of all rightly classified positive samples to the total sample's count. The mathematical formulas of these measurements can be expressed as [68,69].

$$Accuracy(\%) = \frac{TP + FP}{TP + TN + FP + FN} \qquad (5)$$

$$Sensitivity(\%) = \frac{TP}{TP + FN} \qquad (6)$$

$$Specificity(\%) = \frac{TN}{TN + FP} \qquad (7)$$

where TP, TN, FP and FN stand for true positive, true negative, false positive and false negative, respectively.

3. Result and discussion

We develop a hybrid model to classify obesity levels from rod, maximal combined and cone responses of ERG signals recommended by ISCEV. For this aim, we firstly apply feature extracting process based on DWT for three different responses taken from both right and left eyes. During this process, the approximation and detail coefficients have been calculated by using fourth-level Daubechies (db4) wavelet. The calculated coefficients for both eyes of normal and obese subjects as example are presented in Fig. 4 and 5, respectively.

Then, the large size coefficients obtained as a result of feature extraction performed with DWT for each ERG response are reduced by using six different statistical properties (the mean absolute value (μ), average power (λ), standard deviation (σ), skewness (ϕ), kurtosis (φ) of the signal coefficients in every sub-band

İ.S. Yapici, O. Erkaymaz and R.U. Arslan

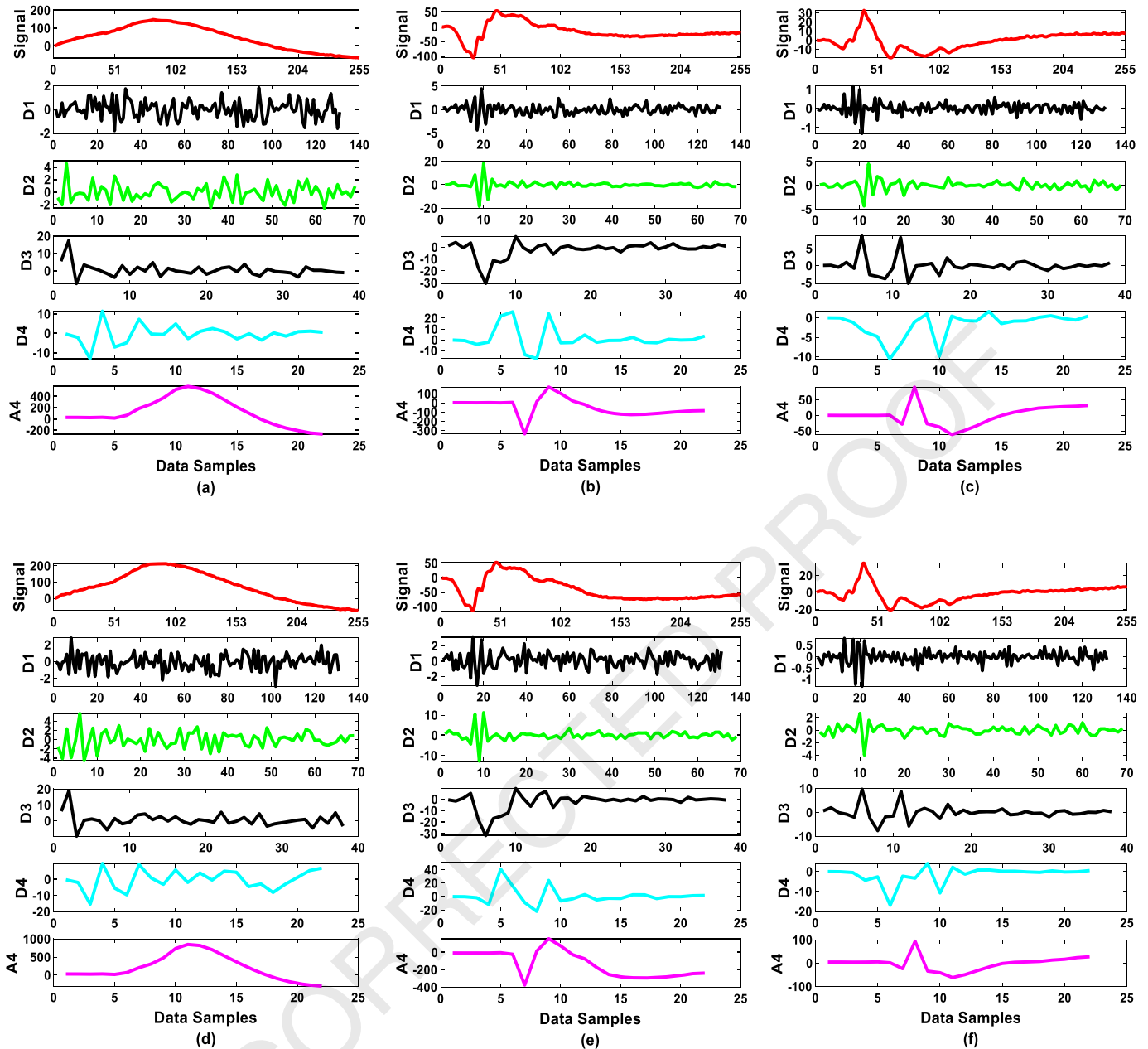*Physics Letters A* ••• (••••) ••••••

Fig. 5. The DWT coefficients obtained from db4 of obese ERG signal; (a) rod response of the right eye, (b) maximal combined response of the right eye, (c) cone response of the right eye, (d) rod response of the left eye, (e) maximal combined response of the left eye, (f) cone response of the left eye.

and ratio of the absolute mean (χ) values of signal coefficients of adjacent sub-bands). Thus, we have designed a dataset with 29 features obtained from statistical properties for each ERG signal. A basic ANN model consisting of the one input, one hidden layer and one output layers using these properties as input is created. Then, we apply training process on ANN model created with 29-H-1 architecture by using $H = 8 \ldots 20$ for designed dataset with 80% training data, 20% testing data. The neuron number of hidden layer is calculated separately for rod, maximal combined and cone responses of ERG signals recorded from both eye. The results are presented in Fig. 6.

As seen Fig. 6, for right eye, basic ANN architecture is 29-12-1, 29-8-1 and 29-10-1 for rod, maximal combined and cone responses, respectively. Besides, for left eye, basic architectures of rod, maximal combined and cone responses are, in turn, 29-14-1, 29-8-1 and 29-18-1.

After the best ANN topologies are acquired for each ERG responses of left and right eyes, we analyze performances of these ANN architectures with the dataset randomly divided into ratio of 80 : 20 for training and testing, respectively, by running 100 trials. The statistical performances of the designed models for classifying the obesity levels for each ERG response are computed. Finally, we apply PSO optimization process on the network topologies and calculate the best ANN parameters (weights and biases) of the networks. The networks optimized with PSO are analyzed with the designed dataset. Statistical performance results for both ANN and PSO optimized ANN (ANN-PSO) are given for both eyes in Tables 2–4.

For the rod response in right eye (Table 2), the ANN model shows more successful results (average accuracy = 93.62%) in the classification of the obesity levels towards normal (85.11%) and overweight subjects (82.98%). The ANN-PSO model exhibits
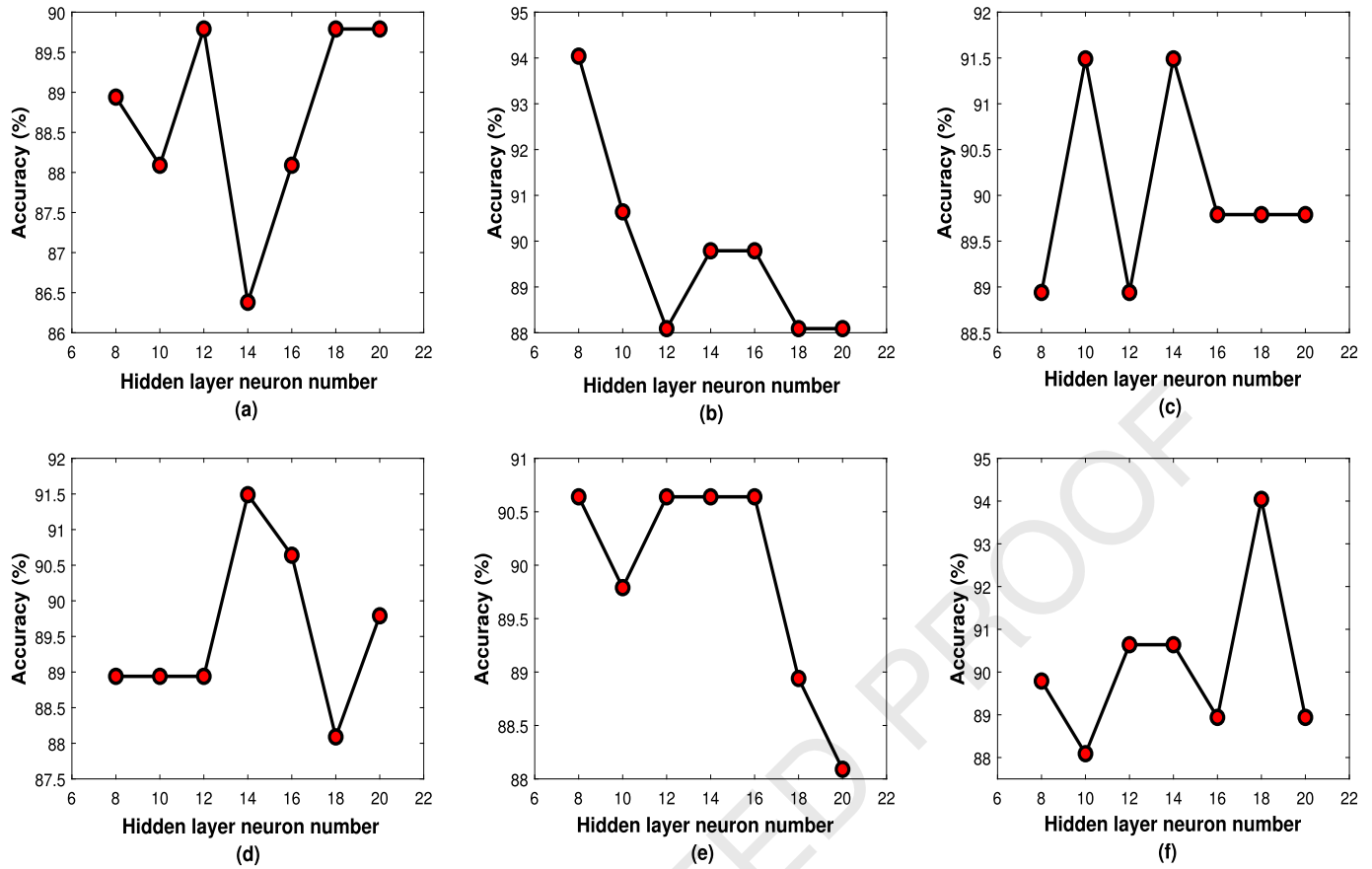
Fig. 6. The simulation results of topology determination process; (a) rod response of the right eye, (b) maximal combined response of the right eye, (c) cone response of the right eye, (d) rod response of the left eye, (e) maximal combined response of the left eye, (f) cone response of the left eye.

Table 2
Statistical performance of ANN-PSO model for rod response of both eyes.

	Number of hidden layer neuron	Obesity classes	Sensitivity (%)	Specificity (%)	Accuracy (%)
Right eye					
ANN	12	Normal	60	97.30	85.11
		Overweight	60	91.89	82.98
		Obese	90	89.19	95.74
		Morbid obese	80	89.19	93.62
		Super obese	85.71	95.45	91.49
		Average	**75.14**	**93.64**	**84.79**
ANN-PSO	12	Normal	90	89.19	89.36
		Overweight	80	97.30	93.62
		Obese	70	97.30	91.49
		Morbid obese	80	91.89	89.36
		Super obese	85.71	100	97.87
		Average	**81.14**	**95.14**	**92.34**
Left eye					
ANN	14	Normal	80	83.78	82.98
		Overweight	70	97.30	91.49
		Obese	70	100	93.62
		Morbid obese	90	97.30	95.74
		Super obese	85.71	95	93.62
		Average	**79.14**	**94.68**	**91.49**
ANN-PSO	14	Normal	70	100	93.62
		Overweight	70	94.59	89.36
		Obese	90	97.30	95.74
		Morbid obese	100	94.59	95.74
		Super obese	85.71	92.50	91.49
		Average	**83.14**	**95.80**	**93.19**

Table 3
Statistical performance of ANN-PSO model for maximal combined response of both eyes.

	Number of hidden layer neuron	Obesity classes	Sensitivity (%)	Specificity (%)	Accuracy (%)
Right eye					
ANN	8	Normal	80	100	95.74
		Overweight	90	94.59	93.62
		Obese	90	94.59	93.62
		Morbid obese	80	100	95.74
		Super obese	85.71	92.50	91.49
		Average	**85.14**	**96.34**	**94.04**
ANN-PSO	8	Normal	80	97.30	93.62
		Overweight	90	97.30	95.74
		Obese	90	89.19	89.36
		Morbid obese	80	100	95.74
		Super obese	100	100	100
		Average	**88**	**96.76**	**94.89**
Left eye					
ANN	8	Normal	80	89.19	87.23
		Overweight	90	94.59	93.62
		Obese	100	97.30	97.87
		Morbid obese	50	94.59	85.11
		Super obese	57.14	95	89.36
		Average	**75.43**	**94.14**	**90.64**
ANN-PSO	8	Normal	60	97.30	89.36
		Overweight	80	94.59	91.49
		Obese	90	89.19	89.36
		Morbid obese	80	94.59	91.49
		Super obese	85.71	97.50	95.74
		Average	**79.14**	**94.64**	**91.49**

Table 4
Statistical performance of ANN-PSO model for cone response of both eyes.

	Number of hidden layer neuron	Obesity classes	Sensitivity (%)	Specificity (%)	Accuracy (%)
Right eye					
ANN	10	Normal	100	86.49	89.36
		Overweight	60	94.59	94.59
		Obese	70	94.59	89.36
		Morbid obese	90	97.309	95.74
		Super obese	71.43	100	95.74
		Average	**78.29**	**94.59**	**91.49**
ANN-PSO	10	Normal	80	100	95.74
		Overweight	100	91.89	93.62
		Obese	90	91.89	91.49
		Morbid obese	80	97.30	93.62
		Super obese	71.43	100	95.74
		Average	**84.29**	**96.22**	**94.04**
Left eye					
ANN	18	Normal	100	97.30	97.87
		Overweight	90	100	97.87
		Obese	80	94.59	91.49
		Morbid obese	70	94.59	89.36
		Super obese	85.71	95	93.62
		Average	**85.14**	**96.30**	**94.04**
ANN-PSO	18	Normal	100	94.59	95.74
		Overweight	80	94.59	91.49
		Obese	80	97.30	93.62
		Morbid obese	100	100	100
		Super obese	85.71	100	97.87
		Average	**89.14**	**97.30**	**95.74**

better performance above average accuracy (92.34%) in the prediction of overweight (93.62%), obese (91.49%) and super obese (97.87%) subjects in respect to normal and morbid obese subjects (89.36%).

On the other hand, in the rod response of the left eye, the ANN model similarly gives more successful results (average accuracy = 94.33%) in classification of the obesity levels in accordance with normal (85.11%) and overweight subjects (82.98%). The ANN-PSO

model also presents more successful results (average accuracy = 94.32%) in classifying of obesity levels towards normal (93.62%) and overweight subjects (89.36%).

For the maximal combined response in right eye (Table 3), the ANN model shows best performance for normal and morbid obese subjects (95.74%) and also presents performance below average accuracy (94.04%) for overweight (93.62%), obese (93.62%) and super obese (91.49%) subjects. Performance of the ANN-PSO model for normal (93.62%) and obese (89.36%) subjects are acquired below average accuracy (94.89%). For the maximal combined response in left eye, the ANN model has above average accuracy performance (90.64%) to classify overweight (93.62%) and obese (97.87%) subjects, the ANN-PSO model has below average accuracy (91.49%) performance for normal and obese subjects (89.36%).

For the cone response in right eye (Table 4), the ANN model shows best performance for morbid and super obese subjects (95.74%) and also exhibits performance below average accuracy (91.49%) for normal (89.36%), overweight (87.23%) and obese (89.36%) subjects. Performance of the ANN-PSO model for normal and super obese subjects (95.74%) are observed above average accuracy (94.04%). On the other hand, in the cone response of left eye, the ANN model has above average accuracy performance (94.04%) to classify of normal and overweight subjects (97.87%), whereas the ANN-PSO model has below average accuracy (95.74%) performance for overweight (91.49%) and obese (93.62%) subjects.

4. Conclusion and discussion

To diagnose obesity levels efficiently, this study has introduced an automated decision support system model by using electroretinogram signals since BMI is not a sufficient criterion to determine the obesity. Contrary to general approaches based on BMI in the literature, it has been shown that obesity can be predictable of the obesity levels from rod, maximal combined and cone responses of electroretinogram signals. To this aim, we firstly analysis electroretinogram signals responses with DWT and then, design ANN and hybrid ANN-PSO models.

Results show that hybrid ANN-PSO model exhibits more robust character than traditional ANN model in discriminating the five different classes of obesity by using from rod, maximal combined and cone responses of electroretinogram signals. In compared with ANN model performance, the hybrid model increases about 2% of classifying score in rod response of both eyes (92.76% of average accuracy). The model enhances about 0.1% and 1% of classifying score in maximal combined response of right (94.89% of average accuracy) and left (91.49% of average accuracy) eyes, respectively. In cone response, the classifying score is obtained about 4.

In sum, the proposed hybrid model shows that the obesity levels can be effectively detected from there different electroretinogram signal responses. In addition, the cone responses are more proper than other responses (rod and maximal combined responses) to classify of disease from electroretinogram signals.

The main advantage of the current study is that classification of obesity levels is carried out by using ERG responses. Therefore it is proved that obesity is related with ERG. On the other hand, the limitation of the study includes lack of data. The designed model must be analyzed on the greater dataset including a wider age range, because the obesity is encountered at almost all ages. As future work, different classification methods will be analyzed with new features to obtain more accuracy performance.

CRediT authorship contribution statement

Irem S. Yapici: Investigation; analytical calculations; Writing – original draft. **Okan Erkaymaz**: Analytical calculations; Writing –

original draft; review editing; Supervision. **Rukiye U. Arslan**: Investigation; Conceptualization; Writing – original draft; review editing; Supervision.

Declaration of competing interest

The authors declare that they have no known competing financial interests or personal relationships that could have appeared to influence the work reported in this paper.

Acknowledgements

References

[1] I. Kalan, Y. Yeşil, Obezite ile ilişkili kronik hastalıklar, Diyabet ve Obezite 78 (2010).

[2] A.M. Yahiro, B.C. Wingo, S. Kunwor, J. Parton, A.C. Ellis, Classification of obesity, cardiometabolic risk, and metabolic syndrome in adults with spinal cord injury, J. Spinal Cord Med. 43 (4) (2020) 485–496.

[3] E.G. Plaza, P.N. López, Application of the wavelet packet transform to vibration signals for surface roughness monitoring in cnc turning operations, Mech. Syst. Signal Process. 98 (2018) 902–919.

[4] F. Bianchini, R. Kaaks, H. Vainio, Weight control and physical activity in cancer prevention, Obes. Rev. 3 (1) (2002) 5–8.

[5] E.E. Calle, C. Rodriguez, K. Walker-Thurmond, M.J. Thun, Overweight, obesity, and mortality from cancer in a prospectively studied cohort of us adults, N. Engl. J. Med. 348 (17) (2003) 1625–1638.

[6] R.H. Eckel, R.M. Krauss, American heart association call to action: obesity as a major risk factor for coronary heart disease, Circulation 97 (21) (1998) 2099–2100.

[7] S.M. Grundy, Metabolic complications of obesity, Endocrine 13 (2) (2000) 155–165.

[8] H. Dw, James wp. obesity, Lancet 9492 (2005) 1197–1209.

[9] V.J. Lawrence, P.G. Kopelman, Medical consequences of obesity, Clin. Dermatol. 22 (4) (2004) 296–302.

[10] F. Sunyer, Medical hazard of obesity, Ann. Intern. Med. 119 (7) (1993) 655–660.

[11] A. Tanikawa, K. Suzuki, R. Nomura, H. Tanaka, T. Mizuguchi, Y. Shimada, M. Horiguchi, The influence of mild cataract on ISCEV standard electroretinogram recorded from mydriatic eyes, Documenta Ophthalmol. (2020) 1–7.

[12] AREDSR Group, Risk factors associated with age-related nuclear and cortical cataract: a case-control study in the age-related eye disease study, AREDS report no. 5, Ophthalmology 108 (8) (2001) 1400.

[13] AREDSR Group, Risk factors associated with age-related macular degeneration: a case-control study in the age-related eye disease study: age-related eye disease study report number 3, Ophthalmology 107 (12) (2000) 2224–2232.

[14] N. Chaturvedi, A.-K. Sjoelie, M. Porta, S.J. Aldington, J.H. Fuller, M. Songini, E.M. Kohner, Markers of insulin resistance are strong risk factors for retinopathy incidence in type 1 diabetes: the eurodiab prospective complications study, Diabetes Care 24 (2) (2001) 284–289.

[15] T.E. Clemons, R.C. Milton, R. Klein, J.M. Seddon, F.L. Ferris 3rd, Risk factors for the incidence of advanced age-related macular degeneration in the age-related eye disease study (AREDS) AREDS report no. 19, Ophthalmology 112 (4) (2005) 533–539.

[16] P. Foster, T. Wong, D. Machin, G. Johnson, S. Seah, Risk factors for nuclear, cortical and posterior subcapsular cataracts in the Chinese population of Singapore: the Tanjong Pagar Survey, Br. J. Ophthalmol. 87 (9) (2003) 1112–1120.

[17] M. Henricsson, L. Nyström, G. Blohmé, J. Östman, C. Kullberg, M. Svensson, A. Schölin, H.J. Arnqvist, E. Björk, J. Bolinder, et al., The incidence of retinopathy 10 years after diagnosis in young adult people with diabetes: results from the nationwide population-based diabetes incidence study in Sweden (diss), Diabetes Care 26 (2) (2003) 349–354.

[18] R. Hiller, M.J. Podgor, R.D. Sperduto, L. Nowroozi, P.W. Wilson, R.B. D'Agostino, T. Colton, T.F.E.S. Group, A longitudinal study of body mass index and lens opacities: the Framingham studies, Ophthalmology 105 (7) (1998) 1244–1250.

[19] P. Gasser, D. Stümpfig, A. Schötzau, U. Ackermann-Liebrich, J. Flammer, Body mass index in glaucoma, J. Glaucoma 8 (1) (1999) 8–11.

[20] B.E. Klein, R. Klein, K.E. Lee, S.C. Jensen, Measures of obesity and age-related eye diseases, Ophthalmic Epidemiol. 8 (4) (2001) 251–262.

[21] T.-M. Kuang, S.-Y. Tsai, W.-M. Hsu, C.-Y. Cheng, J.-H. Liu, P. Chou, Body mass index and age-related cataract: the Shihpai eye study, Arch. Ophthalmol. 123 (8) (2005) 1109–1114.

[22] D.A. Schaumberg, W.G. Christen, S.E. Hankinson, R.J. Glynn, Body mass index and the incidence of visually significant age-related maculopathy in men, Arch. Ophthalmol. 119 (9) (2001) 1259–1264.

[23] M.C. Leske, A. Connell, S.-Y. Wu, L.G. Hyman, A.P. Schachat, Risk factors for open-angle glaucoma: the Barbados eye study, Arch. Ophthalmol. 113 (7) (1995) 918–924.

[24] C. Younan, P. Mitchell, R. Cumming, E. Rochtchina, J. Panchapakesan, K. Tumuluri, Cardiovascular disease, vascular risk factors and the incidence of cataract and cataract surgery: the blue Mountains eye study, Ophthalmic Epidemiol. 10 (4) (2003) 227–240.

[25] J.M. Seddon, J. Cote, N. Davis, B. Rosner, Progression of age-related macular degeneration: association with body mass index, waist circumference, and waist-hip ratio, Arch. Ophthalmol. 121 (6) (2003) 785–792.

[26] H.A. Van Leiden, J.M. Dekker, A.C. Moll, G. Nijpels, R.J. Heine, L.M. Bouter, C.D. Stehouwer, B.C. Polak, Blood pressure, lipids, and obesity are associated with retinopathy: the Hoorn study, Diabetes Care 25 (8) (2002) 1320–1325.

[27] N. Cheung, T.Y. Wong, Obesity and eye diseases, Surv. Ophthalmol. 52 (2) (2007) 180–195.

[28] M.F. Marmor, G.E. Holder, M.W. Seeliger, S. Yamamoto, Standard for clinical electroretinography (2004 update), Doc. Ophthalmol. 108 (2) (2004) 107–114.

[29] F.Ç. Gündoğan, Ü. Erdem, G. Sobacı, M.Z. Bayraktar, Desen elektroretinogram (perg) normal değerlerimiz, Gülhane TD 48 (1) (2006) 19–21.

[30] F.Ç. Gündoğan, Ü. Erdem, M.Ş. Hamurcu, G. Sobacı, M.Z. Bayraktar, Flaş elektroretinogram (ferg) normal değerlerimiz, Gülhane Tıp Dergisi 48 (1) (2006) 14–18.

[31] J.M. Miguel-Jiménez, S. Ortega, L. Boquete, J.M. Rodríguez-Ascariz, R. Blanco, Multifocal erg wavelet packet decomposition applied to glaucoma diagnosis, Biomed. Eng. Online 10 (1) (2011) 1–13.

[32] N. Öztürk, M.K. Gündüz, M. Okka, Patern elektroretinografide normal değerler, Retina-Vitrеus/J. Retina-Vitreous 23 (3) (2015) 231–236.

[33] R. Barraco, D.P. Adorno, M. Brai, An approach based on wavelet analysis for feature extraction in the a-wave of the electroretinogram, Comput. Methods Programs Biomed. 104 (3) (2011) 316–324.

[34] N.J. Nadolski, C.X. Wong, J.C. Hocking, Electroretinogram analysis of zebrafish retinal function across development, Doc. Ophthalmol. (2020) 1–11.

[35] M. Gauvin, J.-M. Lina, P. Lachapelle, Advance in erg analysis: from peak time and amplitude to frequency, power, and energy, BioMed Res. Int. 2014 (2014) 1–11.

[36] R. Barraco, D.P. Adorno, M. Brai, L. Tranchina, A comparison among different techniques for human erg signals processing and classification, Phys. Med. 30 (1) (2014) 86–95.

[37] R. Barraco, D.P. Adorno, M. Brai, Wavelet analysis of human photoreceptoral response, in: 2010 3rd International Symposium on Applied Sciences in Biomedical and Communication Technologies, ISABEL 2010, IEEE, 2010, pp. 1–4.

[38] A.M. Alaql, Analysis and Processing of Human Electroretinogram, The University of South, Florida, 2016.

[39] H. Zhang, B.S. Sajdak, D.K. Merriman, M.A. McCall, J. Carroll, D.M. Lipinski, Electroretinogram of the cone-dominant thirteen-lined ground squirrel during euthermia and hibernation in comparison with the rod-dominant brown Norway rat, Investig. Ophthalmol. Vis. Sci. 61 (6) (2020) 6.

[40] O. Erkaymaz, İ.S. Yapici, R.U. Arslan, Effects of obesity on time-frequency components of electroretinogram signal using continuous wavelet transform, Biomed. Signal Process. Control 66 (2021) 102398.

[41] A. Güven, S. Kara, Diagnosis of the macular diseases from pattern electroretinography signals using artificial neural networks, Expert Syst. Appl. 30 (2) (2006) 361–366.

[42] S. Kara, A. Güven, Training a learning vector quantization network using the pattern electroretinography signals, Comput. Biol. Med. 37 (1) (2007) 77–82.

[43] K. Polat, S. Kara, A. Güven, S. Güneş, A hybrid automated detection system based on least square support vector machine classifier and k-nn based weighted pre-processing for diagnosing of macular disease, in: International Conference on Adaptive and Natural Computing Algorithms, Springer, 2007, pp. 338–345.

[44] J. Miguel-Jiménez, S. Ortega, L. Boquete, J. Rodríguez-Ascariz, R. Blanco, Multifocal electroretinography: structural pattern analysis and early glaucoma detection, Electron. Lett. 45 (22) (2009) 1113–1115.

[45] L. Boquete, J.M. Miguel-Jiménez, S. Ortega, J. Rodríguez-Ascariz, C. Pérez-Rico, R. Blanco, Multifocal electroretinogram diagnosis of glaucoma applying neural networks and structural pattern analysis, Expert Syst. Appl. 39 (1) (2012) 234–238.

[46] A. Bagheri, D.P. Adorno, P. Rizzo, R. Barraco, L. Bellomonte, Empirical mode decomposition and neural network for the classification of electroretinographic data, Med. Biol. Eng. Comput. 52 (7) (2014) 619–628.

[47] S. Kara, A. Güven, A.Ö. Öner, Utilization of artificial neural networks in the diagnosis of optic nerve diseases, Comput. Biol. Med. 36 (4) (2006) 428–437.

[48] J.M. Miguel-Jiménez, R. Blanco, L. De-Santiago, A. Fernandez, J. Rodriguez-Ascariz, R. Barea, J. Martin-Sanchez, C. Amo, E. Sanchez-Morla, L. Boquete, Continuous-wavelet-transform analysis of the multifocal erg waveform in glaucoma diagnosis, Med. Biol. Eng. Comput. 53 (9) (2015) 771–780.

[49] R. Ross, I.J. Neeland, S. Yamashita, I. Shai, J. Seidell, P. Magni, R.D. Santos, B. Arsenault, A. Cuevas, F.B. Hu, et al., Waist circumference as a vital sign in clinical practice: a consensus statement from the ias and iccr working group on visceral obesity, Nat. Rev. Endocrinol. 16 (3) (2020) 177–189.

[50] D. Okorodudu, M. Jumean, V.M. Montori, A. Romero-Corral, V. Somers, P. Erwin, F. Lopez-Jimenez, Diagnostic performance of body mass index to identify obesity as defined by body adiposity: a systematic review and meta-analysis, Int. J. Obes. 34 (5) (2010) 791–799.

[51] A.N.C. Gungor, M. Asik, N. Unsal, A. Seven, M. Ozekinci, N.K. Duru, A. Ergn, Is BMI sufficient to evaluate the association between obesity and ovarian reserves?, Int. J. Gynecol. Obstet. Neonatal Care 1 (1) (2014) 14–18.

[52] J. Yang, V.V. Govindaraj, M. Yang, S.-H. Wang, Hearing loss detection by discrete wavelet transform and multi-layer perceptron trained by nature-inspired algorithms, Multimed. Tools Appl. (2020) 1–29.

[53] R.X. Gao, R. Yan, Wavelets: Theory and Applications for Manufacturing, Springer Science & Business Media, 2010.

[54] S.S. Nair, K.P. Joseph, Wavelet based electroretinographic signal analysis for diagnosis, Biomed. Signal Process. Control 9 (2014) 37–44.

[55] J.N. Weiss, Treatment of central retinal vein occlusion by injection of tissue plasminogen activator into a retinal vein, Am. J. Ophthalmol. 126 (1) (1998) 142–144.

[56] S.G. Mallat, A theory for multiresolution signal decomposition: the wavelet representation, IEEE Trans. Pattern Anal. Mach. Intell. 11 (7) (1989) 674–693.

[57] A. Subasi, S. Jukic, J. Kevric, Comparison of EMD, DWT and WPD for the localization of epileptogenic foci using random forest classifier, Measurement 146 (2019) 846–855.

[58] J. Kevric, A. Subasi, Comparison of signal decomposition methods in classification of eeg signals for motor-imagery bci system, Biomed. Signal Process. Control 31 (2017) 398–406.

[59] M. Bayatvarkeshi, K. Mohammadi, O. Kisi, R. Fasihi, A new wavelet conjunction approach for estimation of relative humidity: wavelet principal component analysis combined with ann, Neural Comput. Appl. 32 (9) (2020) 4989–5000.

[60] R. Uzun, O. Erkaymaz, I.S. Yapici, Comparison of artificial neural network and regression models to diagnose of knee disorder in different postures using surface electromyography, Gazi Univ. J. Sci. 31 (1) (2018) 100–110.

[61] O. Erkaymaz, M. Ozer, Impact of small-world network topology on the conventional artificial neural network for the diagnosis of diabetes, Chaos Solitons Fractals 83 (2016) 178–185.

[62] O. Erkaymaz, M. Ozer, M. Perc, Performance of small-world feedforward neural networks for the diagnosis of diabetes, Appl. Math. Comput. 311 (2017) 22–28.

[63] C. Kaya, O. Erkaymaz, O. Ayar, M. Özer, Determination of the physiological effects of diabetic retinopathy disease from video-oculography (VOG) signals using discrete wavelet transform, in: 2016 Medical Technologies National Congress, TIPTEKNO, IEEE, 2016, pp. 1–4.

[64] C. Kaya, O. Erkaymaz, O. Ayar, M. Özer, Impact of hybrid neural network on the early diagnosis of diabetic retinopathy disease from video-oculography signals, Chaos Solitons Fractals 114 (2018) 164–174.

[65] O. Erkaymaz, Resilient back-propagation approach in small-world feed-forward neural network topology based on Newman–Watts algorithm, Neural Comput. Appl. 32 (20) (2020) 16279–16289.

[66] O. Erkaymaz, Fonksiyon yaklaşımı probleminde esnek küçük-dünya ağlarının topolojik değişiminin performansa etkisi, El-Cezeri J. Sci. Eng. 7 (3) (2020) 1398–1406.

[67] S. Gambhir, S.K. Malik, Y. Kumar, Pso-ann based diagnostic model for the early detection of Dengue disease, New. Horizons Transl. Medicine 4 (1–4) (2017) 1–8.

[68] R.U. Arslan, Y. İşler, M. Toksan, Prediction of the success of wart treatment methods, Contracampo 39 (1) (2020) 44–52.

[69] R.O. Duda, P.E. Hart, et al., Pattern Classification, John Wiley & Sons, 2006.